DIRECT NUMERICAL SIMULATION OF ROUGH WALL OPEN CHANNEL FLOW

Clemens Chan-Braun
Institute of Hydromechanics
Karlsruhe Institute of Technology
Kaiserstrasse 12, 76131 Karlsruhe
chan-braun@kit.edu

Manuel García-Villalba
Bioingeniería e Ingeniería Aeroespacial
Universidad Carlos III de Madrid
Leganés 28911, Spain
manuel.garcia-villalba@uc3m.es

Markus Uhlmann
Institute of Hydromechanics
Karlsruhe Institute of Technology
Kaiserstrasse 12, 76131 Karlsruhe
uhlmann@kit.edu

ABSTRACT

Direct numerical simulation of flow over one layer of spheres above a rigid wall has been carried out. Two cases are considered. In the first one the spheres are small and the flow is in the hydraulically smooth regime. In the second one, the spheres are approximately three times larger and the flow is in the transitionally rough regime. Various possible definitions of the normalisation parameters are discussed in detail. The instantaneous flow field and the flow statistics are briefly presented. The main focus of the study is on drag and lift acting on the particles, which are studied using 2D probability density functions and temporal correlations.

INTRODUCTION

The present study is motivated by the problem of defining the onset of sediment erosion which is of interest to many aspects of engineering. Examples are the stability of bridge piers or the stability of foundations of off-shore wind turbines which can be considerably weakened by sediment erosion. The design of protection devices for these structures is often based on estimations of the onset of sediment transport, which is generally linked to the force acting on a particle due to the hydrodynamic interaction between flow and boundaries (cf. García, 2008, pp. 47). However, while many publications exist on forces on a single sphere in fluid flow (e.g. Yun et al., 2006; Zeng et al., 2009; Lee and Balachandar, 2010, and literature herein), only a limited number of publications consider the force on a sphere in a rough wall (e.g. Hall, 1988; Singh et al., 2007; Dwivedi et al., 2010). This lack of data might be related to the difficulties of directly measuring the force on a particle in experiments (cf. Muthanna et al., 2005, for a discussion) or the much higher computational costs related to numerical simulations of flow over rough walls compared to flow over smooth walls, i.e. increasing computing power, made simulations of rough walls feasible only in recent years.

Table 1. Setup parameters of simulations; $Re_b = U_{bh}h/\nu$ is the bulk Reynolds number based on the bulk velocity U_{bh}, the effective flow depth $h = H - y_0$ and the kinematic viscosity, ν; $Re_\tau = u_\tau h/\nu$ is the friction Reynolds number, where u_τ is the friction velocity; $D^+ = Du_\tau/\nu$ is the particle diameter in viscous units; $D/\Delta x$ is the resolution of a particle; Δx^+ is the grid spacing in viscous units.

Case	Re_b	Re_τ	D^+	$D/\Delta x$	Δx^+
F10	2870	188	10.7	14	0.77
F50	2880	235	49.3	46	1.07

To provide some high-fidelity data of force on particles and to make a first step towards improving the understanding of the fundamental mechanisms involved in sediment erosion direct numerical simulations of open-channel flow over a layer of fixed particles were carried out. The present paper discusses some aspects of the definition of the scaling parameters, the flow field and the hydrodynamic forces acting on the particles.

NUMERICAL SETUP

The flow configuration consists of turbulent open-channel flow over a geometrically rough wall. The wall is formed by one layer of fixed spheres which are packed in a square arrangement (see Figure 1). The distance between the particle centres is $D + 2\Delta x$, where D is the particle diameter and Δx is the grid spacing. At $y = 0$ a rigid wall is located below the layer of spheres. As can be seen in Figure 1 this rigid wall is roughened by spherical caps staggered in the streamwise and spanwise direction with respect to the layer of

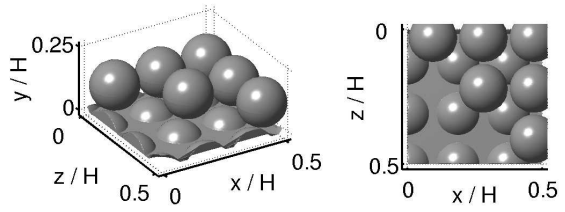

Figure 1. Close-up of particle arrangement on bottom wall in case F50 jointly with solid wall roughened by particle heaps.

spheres above.

The physical and numerical parameters of the simulations are summarised in Table 1. The dimensions of the computational domain are $L_x/H \times L_y/H \times L_z/H = 12 \times 1 \times 3$, in streamwise, wall-normal and spanwise direction, respectively. An equidistant Cartesian grid with $3072 \times 256 \times 768$ grid points is employed. Two cases are considered with different channel-height to sphere-diameter ratio H/D: case F10 with $H/D = 18.3$ and a total of 9216 particles, and case F50 with $H/D = 5.6$ and a total of 1024 particles.

Periodic boundary conditions are applied in streamwise and spanwise directions. At the upper boundary a free-slip condition is employed. At the bottom boundary a no-slip condition is applied. The spheres are resolved using a variant of the immersed boundary technique of (Peskin, 1972, 2002) proposed by Uhlmann (2005). The incompressible Navier-Stokes equations are integrated in time using a standard fractional step method with a semi-implicit discretisation in time and central finite differences in space. Details on the numerical method are provided in Uhlmann (2005, 2008). A more detailed description of the setup can be found in Chan-Braun (2011); Chan-Braun et al. (2011).

As an illustration of the complexity of the flow, snapshots are displayed in Figure 2, which show iso-contours of the instantaneous streamwise velocity fluctuation for both cases. In case F10, the classical arrangement of low speed (blue) and high speed (red) streaks is clearly observed. In that case the spheres are small and the streaks differ little from those observed in the flow over a smooth wall. In case F50 the spheres are roughly three times larger than in case F10, but the overall picture is still similar. However, the streaks seem to be somewhat smaller and small filaments of high and low speed appear to be preferentially aligned in between the particles. The fact that large scale structures are damped with increasing roughness has been previously observed for example by Flores and Jiménez (2006).

DEFINITION OF FRICTION VELOCITY AND POSITION OF VIRTUAL WALL

In analogy to flow over smooth walls, the flows over surfaces roughened by two- or three-dimensional elements might be considered homogeneous in streamwise and spanwise direction for distances far enough from the wall such that the horizontal spatial variances of the time-averaged flow field are small. However, in contrast to smooth walls the origin of the wall-normal coordinate, y_0, cannot be unambiguously defined for rough boundaries. Similarly, the definition of the friction velocity, u_τ, has to be done with care in flows over rough walls, while for smooth walls the definition is straightforward based on the shear stress at the wall τ_w and the density ρ as $u_\tau = \sqrt{\tau_w/\rho}$. Both quantities, y_0 and u_τ, are of interest to scale the results of wall bounded flows and in particular for the comparison between smooth and rough boundaries. In the following we review some of the common definitions for y_0 and u_τ.

A priori definitions of the origin of the wall-normal coordinate, $y0$, can be based on geometrical considerations. Examples are the volume of the roughness elements divided by the area of the virtual wall (cf. Schlichting, 1936), which for the present geometry leads to $y_0/D = 0.44$ (0.56) in case F10 (F50), or the average of the maximum surface elevation, which leads to $y_0/D = 0.54$ (0.65) in case F10 (F50). Here, $y0$ is measured from the rigid wall at $y = 0$ as shown in Figure 1.

A posteriori methods employ the data from measurements or simulations to define y_0. Thom (1971) and Jackson (1981) show that a possible choice is the mean momentum absorption plane, obtained as the centroid of the drag profile on the roughness elements. In the present study such a definition would lead to values of $y_0/D = 0.88$ (0.84) in case F10 (F50). It should be noted that in case of a porous sediment layer, this definition is biased by the inter-porous flow. Most researchers, however, use methods which involve the adjustment of a logarithmic law to the mean velocity profile (Raupach et al., 1991), especially for high Reynolds number flows.

Based on the above methods, several studies on turbulent flow over spheres provide a value of y_0 for a given particle diameter, showing that the variation of y_0/D is in the range 0.68 to 0.82 (cf. reviews in Nezu and Nakagawa, 1993; Dittrich, 1998; Detert et al., 2010; Chan-Braun, 2011). In the present work, the position of the virtual wall was selected to be fixed at a given level $y_0/D = 0.8$ which is inside the range of values determined in relevant experiments.

Turning now to the definition of the velocity scale, u_τ, three common approaches are discussed in the following. Again, a widely used method is to obtain u_τ by adjusting a logarithmic law to the mean velocity profile. Assuming the values $\kappa = 0.4$ and $y_0/D = 0.8$ for the Kármán constant and the offset of the virtual wall, respectively, a fit over the range $50\delta_\nu \leq (y - y_0) \leq 0.5h$ yields $u_\tau/U_{bh} = 0.062$ (0.081) in case F10 (F50). However, it should be recalled that in the present low-Reynolds number flow the limited extent of the logarithmic region makes this approach relatively error-prone.

Alternatively, the global momentum balance can be used in order to relate the driving force (either due to a pressure gradient or gravity) to the different contributions to the drag force generated at the fluid-solid interfaces. While the mean momentum balance is uniquely defined, it does not immediately provide a velocity scale. In some studies the velocity scale is defined from the volumetric force integrated from the virtual wall-distance to the free surface (for example Nakagawa and Nezu, 1977; Detert et al., 2010), i.e. $u_\tau^2 = -\langle \mathrm{d}p_l/\mathrm{d}x \rangle h/\rho$, where h is the effective flow depth, $h = H - y_0$, $\mathrm{d}p_l/\mathrm{d}x$ is the constant pressure gradient and $\langle \cdot \rangle$ refers to averaging in time and wall parallel planes. This definition leads to $u_\tau/U_{bh} = 0.066$ (0.082) in case F10 (F50).

Finally, let us consider definitions based on the total shear stress profile. In smooth-wall flow, the total shear stress

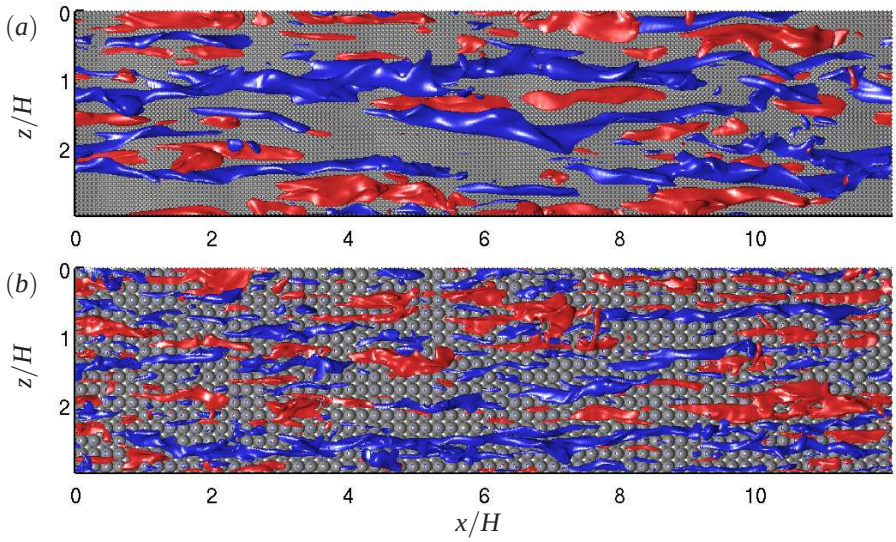

Figure 2. Top view on an instantaneous flow field in case F10 (a) and case F50 (b). Red (blue) surfaces are iso-contours of the streamwise velocity fluctuation at values $+3u_\tau$ ($-3u_\tau$).

τ_{tot} is linear with wall-distance and the appropriate velocity scale is given by $u_\tau^2 = \tau_{tot}(0)/\rho$. In rough-wall flow, τ_{tot} in general deviates from a linear relation below the roughness crests which prevents the use of a similar definition, e.g. based upon $\tau_{tot}(y = y_0)$. Instead, some researchers propose to determine the velocity scale independently of the position of the virtual wall by using the total shear stress at the roughness crests, i.e. $u_\tau^2 = \tau_{tot}(y = D)/\rho$ (Pokrajac et al., 2006). This definition leads to values of $u_\tau/U_{bh} = 0.065$ (0.080) in case F10 (F50). Note that this latter definition makes a direct comparison of different data sets difficult, since the total shear stress profiles $\tau_{tot}/(\rho u_\tau^2)$ represented as a function of $(y-y_0)/h$ will in general not collapse. Alternatively, u_τ can be computed from the total shear stress extrapolated from the region where it varies linearly (i.e. above the roughness crests) down to the position of the virtual wall, yielding the relation

$$\tau_{tot} = u_\tau^2 \left(1 - \frac{y-y_0}{h}\right) \qquad (1)$$

valid for $y > D$. This definition leads to $u_\tau/U_{bh} = 0.066$ (0.082) in case F10 (F50) and has been used in the present study. Incidentally it can be deduced from the global momentum balance that the latter definition implies $u_\tau^2 = -\langle \mathrm{d}p_l/\mathrm{d}x\rangle h/\rho$, i.e. it turns out that the definition of u_τ through (1) is equivalent to the above mentioned definition used by Nakagawa and Nezu (1977) and Detert et al. (2010) based upon an integral of the driving force.

The values obtained for u_τ usig the various methods do not differ much. The largest deviations occur for the case F50. We have checked that the results do not change significantly with a different y_0 in the range of values determined in relevant experiments. As an example, Figure 3 shows mean streamwise velocity profile of case F50 for y_0/D defined in the range of 0.70 to 0.85 in comparison with the smooth wall results. As can be expected, the largest influence can be observed in the vicinity of the rough wall. It can be seen that the influence on the outer flow is small and does not alter conclusions drawn in this study.

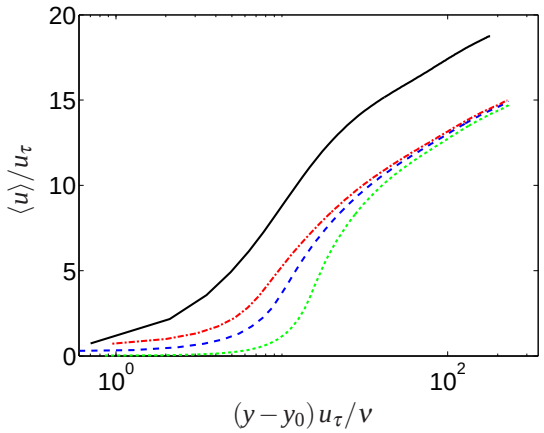

Figure 3. Time and spatially averaged streamwise velocity component $\langle u\rangle$ of case F50 and smooth wall reference case as a function of wall distance. Profiles shown are in semi-logarithmic scale and normalised by ν and u_τ based on three different definition of y_0: — smooth wall reference case ($y_0 = 0$), $-\cdot-$ $y_0/D = 0.7$, $--$ $y/D = 0.8$, $\cdots$ $y_0/D = 0.85$.

RESULTS

Figure 4 shows the mean streamwise velocity profile, $\langle u\rangle/u_\tau$, in case F10 and F50 in comparison with the smooth wall reference case as a function of wall distance. As can be seen the profiles shift with increasing values of D^+ of case F10 to case F50 to smaller values of $\langle u\rangle/u_\tau$. This effect is well known from the literature (cf. Schlichting, 1965, pp. 487), and shows that while the effect of roughness is weak in case F10

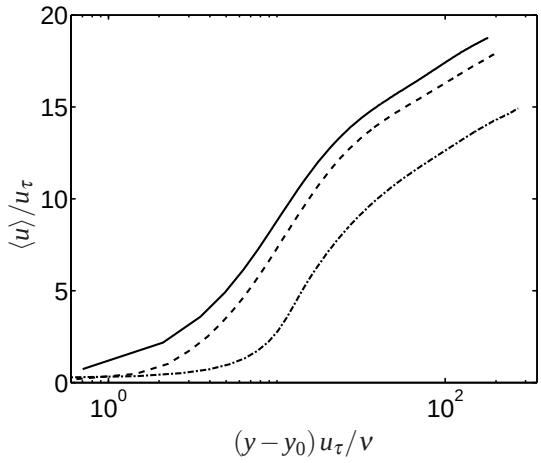

Figure 4. Time and spatially averaged streamwise velocity component $\langle u \rangle$ of case F10 and case F50 in comparison with smooth wall open channel flow simulation; normalised with u_τ as a function of $(y-y_0)u_\tau/\nu$; Lines show — smooth wall reference case, – – case F10, – · – case F50.

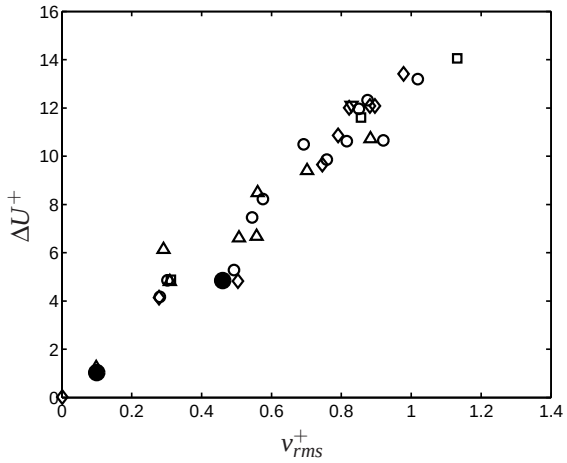

Figure 5. Velocity shift ΔU^+ as a function of the wall-normal velocity fluctuation at the plane positioned at the particles crest, $y = D$. Figure adapted from Orlandi and Leonardi (2008), Burattini et al. (2008), □; Orlandi and Leonardi (2008), ◇; Leonardi et al. (2003), ○; Orlandi and Leonardi (2006), △; Flores and Jiménez (2006), ▽; present simulations, •.

Table 2. Statistics of drag and lift in case F10 and case F50. $C_F^{x_i} = \langle F^{x_i}/F_R \rangle$ is the normalised mean force component in the x_i-direction, with F_R as defined in the text, $\sigma_F^{x_i}$ is the normalised standard deviation of the force in x_i, $S_F^{x_i}$ and $K_F^{x_i}$ are the skewness and kurtosis of the respective force component.

Case	C_F^x	C_F^y	σ_F^x/F_R	σ_F^y/F_R
F10	1.04	0.19	0.57	0.20
F50	1.15	0.37	1.32	0.66
Case	S_F^x	S_F^y	K_F^x	K_F^y
F10	0.18	1.80	10.13	19.08
F50	0.06	0.26	4.98	5.68

it is stronger in case F50. A similar conclusion can be drawn from Figure 5 that shows the shift between the velocity profile in the rough wall case and the reference smooth wall case ΔU^+, as a function of the root mean square of the velocity fluctuation in wall normal direction v_{rms} at $y = D$. In the figure a compilation of data from other experiments is also shown as presented by Orlandi and Leonardi (2008) who argued that there should be a linear relation between ΔU^+ and v_{rms}. The present data support that hypothesis. From the velocity shift and other evidence discussed in more detail in Chan-Braun (2011) and Chan-Braun et al. (2011) it can be concluded that case F10 is in the hydraulically-smooth regime while case F50 is in the transitionally-rough regime.

We concentrate now on the the hydrodynamic forces on the spheres. Table 2 provides the statistics of drag and lift on the particle, normalised by a reference force defined as $F_R = \rho u_\tau^2 A_R$, where A_R is the projected area per particle. In both cases positive mean values for drag and lift are obtained, lift being smaller than the drag by 18% (32%) in case F10 (F50). It should be noted that the obtained values for lift compare well to the study of Hall (1988) (not shown). The standard deviation of drag increases from being larger than the mean drag by a factor of 0.60 in case F10 to a factor of 1.15 larger than the mean drag in case F50. Similarly the values of the standard deviation of lift also increase from a factor of 1.05 of the mean lift in case F10 to 1.78 in case F50. The increase in drag and lift fluctuations with increasing roughness is somewhat surprising as it contradicts to some degree the assumption often made that the force fluctuations directly correlate with the velocity fluctuations in the vicinity of the wall. The fluctuations in streamwise direction however decrease from case F10 to F50 in agreement to the influence of roughness generally reported in the literature (not shown).

The skewness of drag and lift can be discussed jointly with the two-dimensional probability density function (2D-pdf) of drag and lift shown in Figures 7*a* and 7*b*. In case F10, the outer iso-contours are somewhat asymmetric with respect to the x-axis of Figure 7(a). Therefore, positive lift fluctuations occur with a higher probability than negative ones. In contrast to this, the contour appear rather symmetric with respect to the y-axis from which it can be concluded that positive as well as negative drag fluctuations occur with similar probabilities. The effect can be quantified by the skewness provided in Table 2, that shows that the skewness is indeed higher for lift than for drag. Table 2 also shows that the skewness of the respective values of drag and lift are higher in case F10 than in case F50. This can also be deduced from Figure 7 (b) in which the contours are nearly circular. Table 2 also provides the values for the kurtosis of lift and drag which cannot be discussed from the 2d-pdf, since the kurtosis is highly influenced by the tails of the distribution which are not shown in the mentioned figure. In general highest values of the kurtosis

are obtained in case F10 while in case F50 the values are close to those of a Gaussian distribution. It is remarkable, that especially in case F10 very high values are obtained for lift which indicates that lift fluctuations of several standard deviations might occur.

As discussed above, the shape of the pdfs in figures 7*a* and 7*b* is almost symmetric with respect to at least one axis. As a consequence it might be assumed that drag and lift are esentially uncorrelated. However, the cross-correlation coefficient of drag and lift as a function of a time shift τ_{lag}, displayed in Figure 6, shows that while there is indeed virtually no correlation for $\tau_{lag} = 0$, a significant correlation occurs with a certain time delay. The correlation reaches a maximum value for a time lag of $\tau_{lag} U_{bh}/h = 0.192$ (0.237) in case F10 (F50). For comparison, the experimental results of Hofland (2005) and Dwivedi (2010) are also included in Figure 6. These experiments were carried out at significantly higher Reynolds numbers and in case of Hofland (2005) also with non-spherical particles. In spite of this, similar correlations were obtained as in the present numerical simulations. The figure shows that the time lag of the correlation seems to scale in outer flow units. This could indicate that the flow structures that contribute to the correlation between lift and drag have a large scale, of the order of the flow depth, and are convected at a velocity of the order of the bulk velocity.

Turning back to the discussion of the 2D-pdfs, Figures 7*c* and 7*d* show the 2D-pdf between lift and drag but with a shift in time corresponding to the maximum correlation. The overall picture is that low/high drag events correlate with low/high lift events with a time delay. However, for a given level of drag fluctuations a rather broad range of lift fluctuations is present and vice versa.

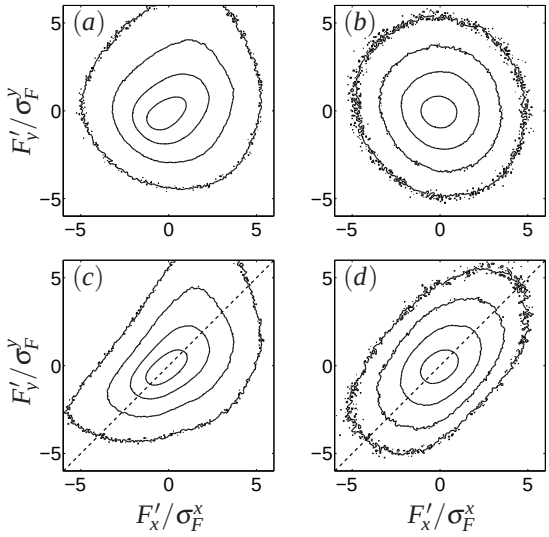

Figure 7. Two-dimensional probability density function (pdf) of drag and lift fluctuations in case F10 (a,c) and F50 (b,d). Panels (a,b) show pdfs with zero time-lag, panels (c,d) show pdfs that maximises the drag-lift $\tau_{lag} U_{bh}/h = 0.192$ (c) in case F10 and $\tau_{lag} U_{bh}/h = 0.237$ (d) in case F50 (cf. figure 6). Lines show iso-contours at a level of probability equal to [1e-4,1e-3,1e-2,1e-1]. The dashed lines in panels (c,d) show relation $F_y'/\sigma_F^y = F_x'/\sigma_F^x$ and are added to guide the eye.

SUMMARY AND CONCLUSION

In this paper, some results of the DNS of flow over one layer of spheres above a rigid wall have been presented. We have discussed several methods available for the specification of y_0 and u_τ in this kind of flows. This issue remains a matter of debate and depends to some extent on the available data in the particular study. However, as long as one of the generally accepted alternatives is adopted, the results will be amenable to physical interpretation, but note that enough information should be provided such that a reader might rescale the results according to an alternative definition of y_0 and u_τ. Flow visualizations have shown the appearance of low and high speed streaks, as expected, whose size seems to be somewhat smaller with increasing roughness. We have also shown that the shift in the mean velocity profile obtained for our cases is consistent with previous experiments and simulations of flow over walls roughened in various geometrical ways. As our main result, the drag and lift on the particles have been discussed. It has been shown that although these two quantities appear to be uncorrelated, this is a misleading observation since temporal correlations show that they are strongly correlated with a time delay. The temporal correlations seem to scale in outer units, a fact supported by comparison to experiments at very different flow conditions.

ACKNOWLEDGEMENTS

This work was supported by the German Research Foundation (DFG) under project JI 18/19-1. The computations have been carried out at the Steinbuch Centre for Computing (SCC) of Karlsruhe Institute of Technology and at the Leibniz Supercomputing Centre (LRZ) of the Bavarian Academy of Sciences and Humanities. The support from these institutions is gratefully acknowledged. We would also like to thank Prof. V. Nikora and Prof. J. Fröhlich and their research groups for active discussions.

REFERENCES

Burattini, P., Leonardi, S., Orlandi, P., and Antonia, R. A. (2008). Comparison between experiments and direct numerical simulations in a channel flow with roughness on one wall. *J. Fluid Mech.*, 600:403–426.

Chan-Braun, C. (2011). *Turbulent open channel flow, sediment erosion and sediment transport*. PhD thesis, Karlsruhe Institute of Technology. in preparation.

Chan-Braun, C., García-Villalba, M., and Uhlmann, M. (2011). Force and torque acting on particles in a transitionally rough open channel flow. submitted.

Detert, M., Nikora, V., and Jirka, G. H. (2010). Synoptic velocity and pressure fields at the water?sediment interface of streambeds. *J. Fluid Mech.*, 660:55–86.

Dittrich, A. (1998). *Wechselwirkung Morphologie/ Strömung naturnaher Fließgewässer*. Habilitation, Universität Karlsruhe (TH).

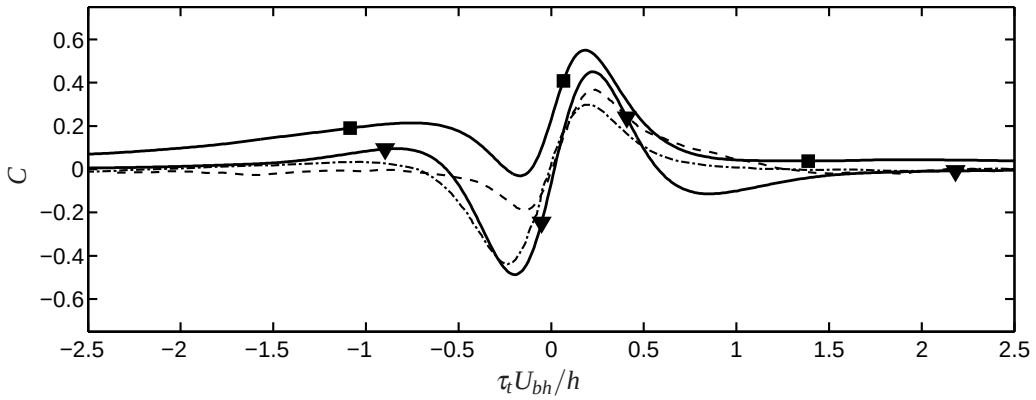

Figure 6. Cross-correlation coefficient as a function of time lag, $\tau_t h/U_{bh}$, of drag and lift fluctuations. The figure shows results of case F10 and case F50 in comparison with the indirect measurements of Hofland (2005) figure 6.5a lowest protrusion at $Re_b = 1.3 \cdot 10^5$, $D^+ = 3300$, (dash-dotted line) and with the direct measurements of Dwivedi (2010) figure 7.23a with zero protrusion at $Re_b = 1.68 \cdot 10^5$, $D^+ = 3100$ (dashed line). Symbols indicate results for case F10, ■; case F50, ▼.

Dwivedi, A. (2010). *Mechanics of sediment entrainment*. Ph.d, The University of Auckland. downloadable at: http://researchspace.auckland.ac.nz.

Dwivedi, A., Melville, B. W., Shamseldin, A. Y., and Guha, T. K. (2010). Drag force on a sediment particle from point velocity measurements: A spectral approach. *Water Resour. Res.*, 46(10):W10529.

Flores, O. and Jiménez, J. (2006). Effect of wall-boundary disturbances on turbulent channel flows. *J. Fluid Mech.*, 566:357–376.

García, M. H. (2008). *Sedimentation engineering: processes, measurements, modeling, and practice*. American Society of Civil Engineers (ASCE), Reston, Va. ASCE Manual of Practice 110.

Hall, D. (1988). Measurements of the mean force on a particle near a boundary in turbulent flow. *J. Fluid Mech.*, 187:451–466.

Hofland, B. (2005). *Rock and Roll, Turbulence-induced damage to granular bed protections*. Ph.d, Technical University Delft. downloadable at: www.library.tudelft.nl → TUDelft publications → Hofland.

Jackson, P. S. (1981). On the displacement height in the logarithmic velocity profile. *J. Fluid Mech.*, 111:15–25.

Lee, H. and Balachandar, S. (2010). Drag and lift forces on a spherical particle moving on a wall in a shear flow at finite Re. *J. Fluid Mech.*, 657:89–125.

Leonardi, S., Orlandi, P., Smalley, R. J., Djenidi, L., and Antonia, R. A. (2003). Direct numerical simulations of turbulent channel flow with transverse square bars on one wall. *J. Fluid Mech.*, 491:229–238.

Muthanna, C., Nieuwstadt, F. T. M., and Hunt, J. C. R. (2005). Measurement of the aerodynamic forces on a small particle attached to a wall. *Exp. Fluids*, 39:455–463.

Nakagawa, H. and Nezu, I. (1977). Prediction of the contributions to the Reynolds stress from bursting events in open-channel flows. *J. Fluid Mech.*, 80(01):99–128.

Nezu, I. and Nakagawa, H. (1993). *Turbulence in Open-Channel Flows*. IAHR/AIRH Monograph Series, Balkema Publishers.

Orlandi, P. and Leonardi, S. (2006). DNS of turbulent channel flows with two- and three-dimensional roughness. *J. Turb.*, 7:1468–5248.

Orlandi, P. and Leonardi, S. (2008). Direct numerical simulation of three-dimensional turbulent rough channels: parameterization and flow physics. *J. Fluid Mech.*, 606:399–415.

Peskin, C. S. (1972). *Flow patterns around heart valves: A digital computer method for solving the equation of motion*. PhD thesis, Albert Einstein College of Medicine.

Peskin, C. S. (2002). The immersed boundary method. *Acta Numerica*, 11:479–517.

Pokrajac, D., Finnigan, J., Manes, C., McEwan, I., and Nikora, V. (2006). On the definition of shear velocity in rough bed open-channel flows. In Ferreiara, R., Alves, E., Leal, J., and Cardoso, A., editors, *River Flow 2006*. A.A. Balkema, Rotterdam.

Raupach, M. R., Antonia, R. A., and Rajagopalan, S. (1991). Rough-wall turbulent boundary layers. *Applied Mechanics Reviews*, 44(1):1–25.

Schlichting, H. (1936). Experimentelle Untersuchungen zum Rauhigkeitsprobem. *Ingenieur Archiv*, 7:1–34.

Schlichting, H. (1965). *Grenzschicht-Theorie*. Verlag G. Braun, Karlsruhe, 5 edition.

Singh, K. M., Sandham, N. D., and Williams, J. J. R. (2007). Numerical simulation of flow over a rough bed. *J. Hydraul. Eng.*, 133(4):386–398.

Thom, A. S. (1971). Momentum absorption by vegetation. *Q.J.R. Meteorol. Soc.*, 97(414):414–428.

Uhlmann, M. (2005). An immersed boundary method with direct forcing for the simulation of particulate flows. *J. Comput. Phys.*, 209(2):448–476.

Uhlmann, M. (2008). Interface-resolved direct numerical simulation of vertical particulate channel flow in the turbulent regime. *Phys. Fluids*, 20(5):053305.

Yun, G., Kim, D., and Choi, H. (2006). Vortical structures behind a sphere at subcritical Reynolds numbers. *Phys. Fluids*, 18(1):015102.

Zeng, L., Najjar, F., Balachandar, S., and Fischer, P. (2009). Forces on a finite-sized particle located close to a wall in a linear shear flow. *Phys. Fluids*, 21(3):033302.